Geophysical Journal International

Geophys. J. Int. (2017) **208,** 424–431
Advance Access publication 2016 October 23
GJI Seismology

doi: 10.1093/gji/ggw402

Effect of soil and bedrock anelasticity on the *S*-wave amplification function

José M. Carcione,[1] Stefano Picotti,[1] Roberto Francese,[2] Massimo Giorgi[1] and Franco Pettenati[1]

[1] *Istituto Nazionale di Oceanografia e di Geofisica Sperimentale - OGS - Borgo Grotta Gigante* 42/c, *I*-34010 *Sgonico (Trieste), Italy.*
E-mail: jcarcione@libero.it
[2] *University of Parma, Parma, Italy*

Accepted 2016 October 21. Received 2016 October 19; in original form 2016 April 20

SUMMARY

We analyse how intrinsic attenuation and bedrock elasticity affect the amplitude and frequency of the resonance peaks of the *S*-wave amplification function. The Zener model (with a single relaxation peak) and the constant-*Q* model are used to describe attenuation. We consider two different cases, namely, the soil is softer than the bedrock (the usual situation, that is, a sediment overlying a stiff formation) and the upper layer is stiffer than the lower half-space (e.g. basalt over sediment). The presence of Zener loss in the upper layer causes a shift of the fundamental peak towards the low frequencies, while no shift is observed due to the non-rigid (viscoelastic) character of the half-space. In the constant-Q case, the shift to the low frequencies is not significant implying that it is difficult to estimate the attenuation parameters on the basis of the location of the resonance peaks. However, attenuation affects the amplitude of the higher modes, while these modes have the same amplitude of the fundamental mode no matter the degree of elasticity of the half-space. Attenuation of the layer and non-rigidity of the half-space affect the peaks, with the latter having a stronger effect. Examples are given, considering two real cases representing a glacier in Northern Italy and an ice stream in the Antarctic continent.

Key words: Amplification function; Anelasticity; Glaciers; *S*-waves.

1 INTRODUCTION

We analyse the effects of soil and bedrock anelasticity on the *S*-wave amplification function, that is, how anelasticity affects the amplitude and frequency of the resonance peaks. The amplification function is an essential concept in the horizontal to vertical spectral ratio (HVSR) method, originally introduced by Nogoshi & Igarashi (1971). The method is based on the frequency spectrum obtained by dividing the horizontal component by the vertical component (H/V ratio), either displacement, particle velocity or acceleration, since the results are equivalent. The source can be ambient noise, earthquakes or active sources of different nature. It has been shown that for shear and Rayleigh waves propagating in a layer over a half-space, the method yields the fundamental resonance frequency and the related amplitude (Lermo & Chávez García 1993; Lunedei & Malischewsky 2015).These investigations suggest that the H/V ratio provides a reliable approximation of the *S*-wave transfer function of a site, if the ratio is controlled by the fundamental Rayleigh waves, there is only an indirect correlation between the H/V peak amplitude and the site amplification (Bonnefoy-Claudet *et al.* 2006). A more detailed study of the influence of surface and body waves by varying several parameters is given in Albarello & Lunedei (2011). A case study is proposed in D'Amico *et al.* (2008), where a first-order reconstruction of the seismic bedrock topography shows a good consistency with available geological/log data.

The first significant and detailed theoretical tests of the method have been performed by Konno & Ohmachi (1998) who show how the H/V ratio is related to the fundamental-mode Rayleigh wave regarding its resonant frequency and to the *S*-wave amplification function. More detailed viscoelastic numerical tests regard the SESAME project, whose results can mainly be found in Bonnefoy-Claudet *et al.* (2006). They have considered 1-D plane-layered models and sources randomly distributed near the surface, that is, impulsive and continuous (machines). The H/V ratio predicts the resonance frequency of the 1-D transfer function corresponding to a vertically incident *S*-wave. Van der Baan (2009) explains the resonances obtained from the H/V ratio as due to *SH* and Love waves but in general these depend on several factors, such as the type of source, medium properties, interface geometry, etc.

The equation used to obtain the amplification function is usually based on a lossless soil overlying a rigid bedrock. Here, we study the effects of soil and bedrock anelasticity on the amplification function of shear waves, that is, the presence of attenuation in the layer and half-space and the fact the latter can be deformable, that is, viscoelastic and not rigid. Kramer (1996) provides the relevant equations of the amplification function, which is the ratio of the

free surface motion amplitude to the bedrock motion amplitude, where viscoelasticity is described by a Kelvin–Voigt solid. Here, we use the Zener and constant-Q models to describe attenuation (e.g. Carcione 2014), a more realistic description for rocks than the Kelvin–Voigt solid, which gives an infinite velocity at high frequencies. More complex models could be used, such as that of Lunedei & Albarello (2015), which considers the whole wavefield or the diffusive wavefield theory (Kawase *et al.* 2011; Sánchez-Sesma *et al.* 2011; García Jerez *et al.* 2013; Kawase *et al.* 2015). However, Kramer's equation satisfactory explains the physics involved in the examples presented here, namely, two real cases representing a glacier in Northern Italy and an ice stream in the Antarctic continent (Picotti *et al.* 2017). Although the theory is applied to glaciers, it can be used for other environments, where the geology can be represented by a flat layer over a half-space, both isotropic and anelastic.

2 SITE AMPLIFICATION FUNCTION

The body S-wave transfer function for a lossy sediment layer (soil) of thickness h over a viscoelastic bedrock describes the ratio of displacement amplitudes between the top and bottom of the layer due to horizontal harmonic motions of the bedrock. Let us define the layer ($i = 1$) and half-space ($i = 2$) complex (Zener) shear wave velocities as v_i, where

$$v = c_R\sqrt{\frac{1+\mathrm{i}\omega\tau a}{1+\mathrm{i}\omega\tau/a}} = c_U\sqrt{\frac{\mathrm{i}\omega\tau+1/a}{\mathrm{i}\omega\tau+a}}, \quad a=\frac{c_U}{c_R}\geq 1, \tag{1}$$

where c_R and c_U are the low (relaxed)- and high (unrelaxed)-frequency limit velocities, ω is the angular frequency, $f = 1/(2\pi\tau)$ is the centre frequency of the relaxation peak and $\mathrm{i} = \sqrt{-1}$. The peak quality factor is given by $Q = 2(1 - 1/a)^{-1}$. Therefore, the properties f, c_U and Q define the media, where $a = Q^{-1} + \sqrt{1 + Q^{-2}}$ (e.g. Carcione 2014). When $c_R = c_U$ we have the lossless case, that is, $a = 1$, $Q = \infty$ and $v = c_U$. We define the lossless case for $\omega \to \infty$, when $v \to c_U$. If $\omega = 0$ we have $v = c_R = c_U/a$.

The transfer function is

$$F(\omega) = \left[\cos\left(\frac{\omega h}{v_1}\right) + \mathrm{i}\left(\frac{\rho_1 v_1}{\rho_2 v_2}\right)\sin\left(\frac{\omega h}{v_1}\right)\right]^{-1} \tag{2}$$

(Takahashi & Hirano 1941; Kramer 1996, eq. 7.26), where ρ_i denotes the mass density. The site amplification function is merely $|F|$. A rigid bedrock is obtained for $\rho_2 v_2 \to \infty$. In this case and in the absence of loss, we have the following resonance frequencies when the cosine vanishes,

$$f_n = (2n+1)f_0, \ n = 0, 1, 2, \ldots, \quad f_0 = \frac{c_{U1}}{4h}. \tag{3}$$

Infinite amplitude values are obtained at these resonance frequencies. An analysis of the transfer function at the fundamental frequency ($n = 0$) is given in Appendix A.

3 RESULTS

We consider two main cases and study the location and amplitude of the fundamental and higher modes. The cases are:

Case 1. The layer (sediment) is softer than the half-space (bedrock) (e.g. sediment over hard rock). 1.1: The impedance contrast is constant and we vary the loss properties. 1.2: The loss properties are constant and we vary the impedance contrast.

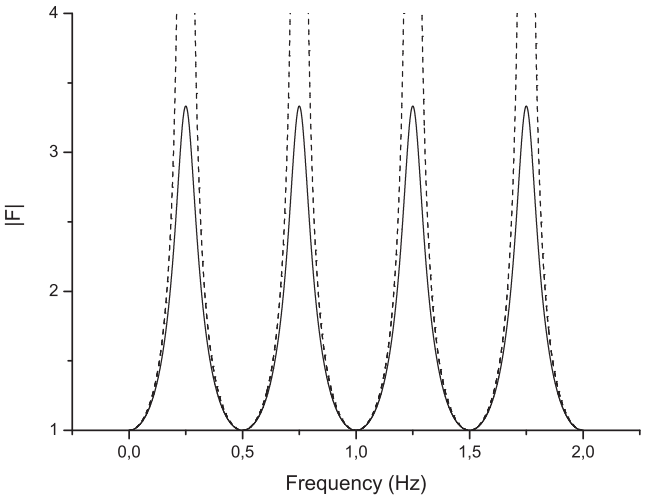

Figure 1. S-wave site amplification in the lossless-elastic (solid line, $Q_1 = \infty$, $\alpha = 0.3$, $Q_2 = 50$) and lossless-rigid (dashed line, $Q_1 = \infty$, $\alpha = 0$) cases.

Case 2. The layer (hard rock) is stiffer than the half-space (sediment) (e.g. basalt over sediment). 2.1: The impedance contrast is constant and we vary the loss properties. 2.2: The loss properties are constant and we vary the impedance contrast.

Let us consider a sediment with $c_{U1} = 1$ km s^{-1}, $\rho_1 = 2$ g cm^{-3}, $Q_1 = 10$ and $h = 1$ km. The impedance contrast is defined as

$$\alpha = \frac{\rho_1 c_{U1}}{\rho_2 c_{U2}}, \tag{4}$$

that is, $\alpha = 0$ yields maximum impedance contrast and $\alpha = 1$ yields no contrast. Note that eq. (2) depends on the lower medium through the impedance $I_2 = \rho_2 c_{U2}$. All the calculations consider $\tau = 1/(2\pi)$, that is, the relaxation peak is centred at a frequency of 1 Hz. In the lossless-rigid case ($Q_1 = \infty$ and $\alpha = 0$), we have $f_n = 0.25$ Hz, 0.75 Hz, 1.25 Hz, 1.75 Hz, ... Generally, the spectra are compared to that of the lossless-rigid case, which is the case mostly used to interpret H/V seismic responses.

3.1 Case 1: soft layer over stiff half-space

Case 1.1. Let us assume $\alpha = 0.3$ and $Q_2 = 50$. The solid and dashed lines in Fig. 1 correspond to the lossless-elastic and lossless-rigid cases, respectively (in this case, $Q_2 = \infty$). The peak in the second case is truncated since it reaches infinite values. The location of the peak is the same in both cases.

The lossy case is given in Fig. 2, where the higher resonances are damped. The comparison of Figs 1 and 2 shows that the presence of loss in the soil produces a shift of the peak towards the left side of the spectrum. If the Zener peak is located at frequencies lower than the fundamental-mode frequency, the shift is smaller, since the resonance peaks 'see' the unrelaxed velocity c_U (the velocity related to the lossless case by definition), while there is a bigger shift if the Zener peak is located at higher frequencies compared to the fundamental one. In this case, the resonance peaks 'see' the relaxed velocity c_R, which is smaller than c_U.

The effects of bedrock elasticity and soil attenuation are similar. A stiffer bedrock means greater amplification as well as a less attenuating soil has the same effect. Fig. 3 compares the lossy and elastic (non-rigid) cases (solid and dashed lines, respectively), where the amplification factor of the fundamental mode is the same. The

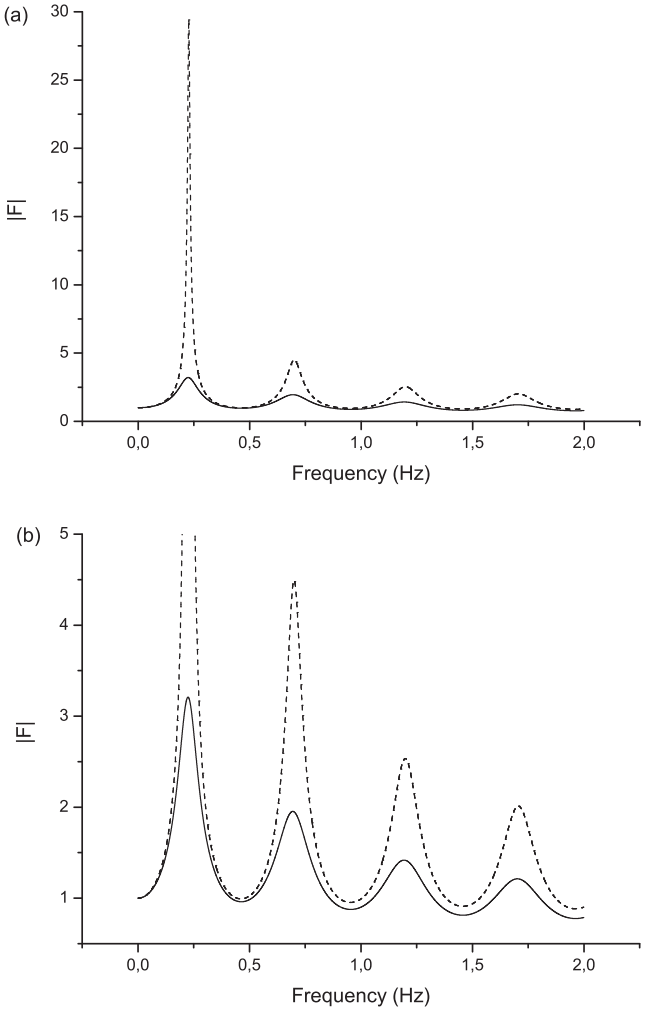

Figure 2. *S*-wave site amplification in the lossy-elastic case (solid line, $Q_1 = 10$, $\alpha = 0.3$, $Q_2 = 50$) and lossy-rigid case (dashed line, $Q_1 = 10$, $\alpha = 0$). Panel (b) shows more details.

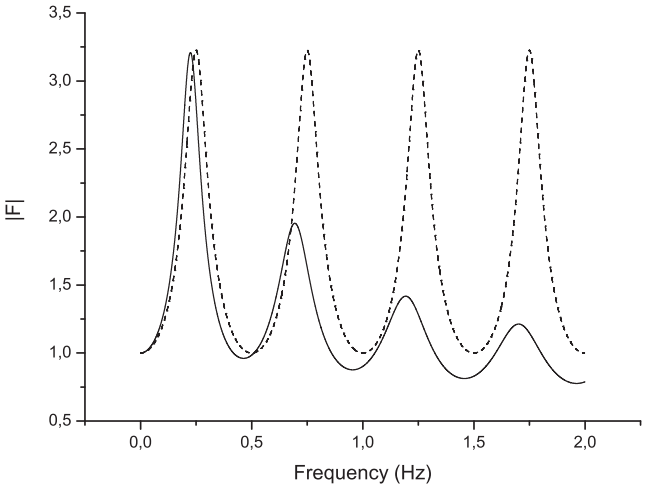

Figure 3. *S*-wave site amplification in the lossy-elastic case (solid line, $Q_1 = 10$, $\alpha = 0.3$, $Q_2 = 50$) and lossless-elastic case (dashed line, $Q_1 = \infty$, $\alpha = 0.31$, $Q_2 = \infty$).

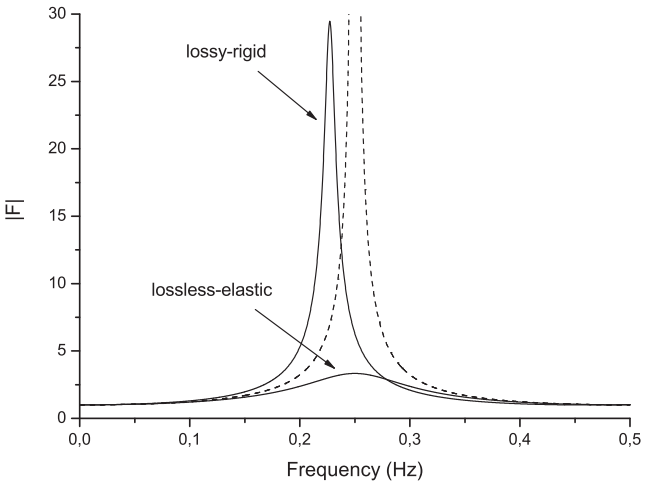

Figure 4. Amplification of the fundamental mode in the lossy-rigid case ($Q_1 = 10$, $\alpha = 0$) and lossless-elastic case ($Q_1 = \infty$, $\alpha = 0.3$, $Q_2 = 50$). The dashed line corresponds to the lossless-rigid case.

effects can be discriminated on the basis of the location of the peak (although there is a small difference) and mainly on the behaviour of the higher modes.

An elastic bedrock has a significant effect on the amplitude as can be seen in Fig. 4, where the curve is compared to the rigid case with attenuation in the sediment. If $Q_1 = 3$ the fundamental mode moves to the left compared to $Q_1 = 10$ as expected and the higher resonances shows a larger shift and stronger attenuation (see Fig. 5). However, the amplitude of the fundamental mode is not affected.

If there is no intrinsic loss, the amplification of the fundamental and higher modes is similar, as can be appreciated in Fig. 3 (dashed line), but the elasticity of the bedrock is a more significant damper of the fundamental mode than intrinsic attenuation, which affects mainly the higher modes (see Fig. 4).

Case 1.2. Let us consider the lossless case ($Q_1 = Q_2 = \infty$) and the lossy case ($Q_1 = 10$, $Q_2 = 50$) and vary the impedance contrast α between 0 (rigid) and 0.8 (very deformable bedrock) in steps of 0.2. The results are shown in Fig. 6. Clearly, the peak location is the same in the lossless case as the impedance contrast varies, while the presence of attenuation implies a shift of the peaks and attenuation of the higher modes.

3.2 Case 2: stiff layer over soft half-space

Case 2.1. The layer is a stiff medium with a density $\rho_1 = 2.5$ g cm^{-3} and $Q_1 = 50$, and the lower half-space has the properties of the soil, that is, $c_{U2} = 1$ km s^{-1} and $\rho_2 = 2$ g cm^{-3}. We assume a constant impedance contrast $\alpha = 2$, so that $c_{U1} = 1.6$ km s^{-1}. Fig. 7 shows the amplification function for the lossless ($Q_2 = \infty$) and lossy cases (dotted and solid lines, respectively). There is damping in the latter case.

Let us assume three values of Q_2, that is, $Q_2 = 10$, 5 and 3. The amplification function shown in Fig. 8(a) does not show significant variations as the Q factor of the half-space decreases. On the other hand, varying the Q factor of the layer and taking $Q_2 = 10$ the curves show remarkable differences (see Fig. 8b).

Case 2.2. The layer is a stiff medium with a density $\rho_1 = 2.5$ g cm^{-3} and $Q_1 = 50$, and the lower half-space has $c_{U2} = 1$ km s^{-1}, $\rho_2 = 2$ g cm^{-3} and $Q_2 = 10$. In this case, we assume the impedance contrast $\alpha = 2$, 5 and 10, such that the velocity of the layer takes the values $c_{U1} = 1.6$, 4 and 8 km s^{-1}, respectively. Fig. 9 shows the amplification function for each value of α. The modes shift to the higher frequencies and the spectrum stretches

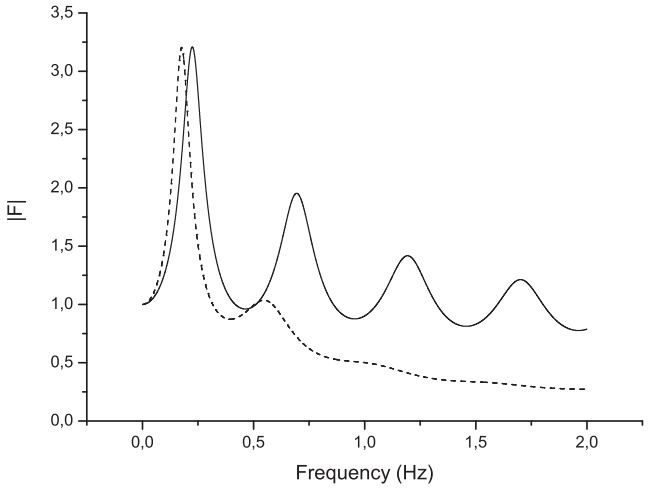

Figure 5. Amplification in the lossy-elastic case ($\alpha = 0.3$) for $Q_1 = 10$ (solid line) and $Q_1 = 3$ (dashed line, $Q_2 = 50$).

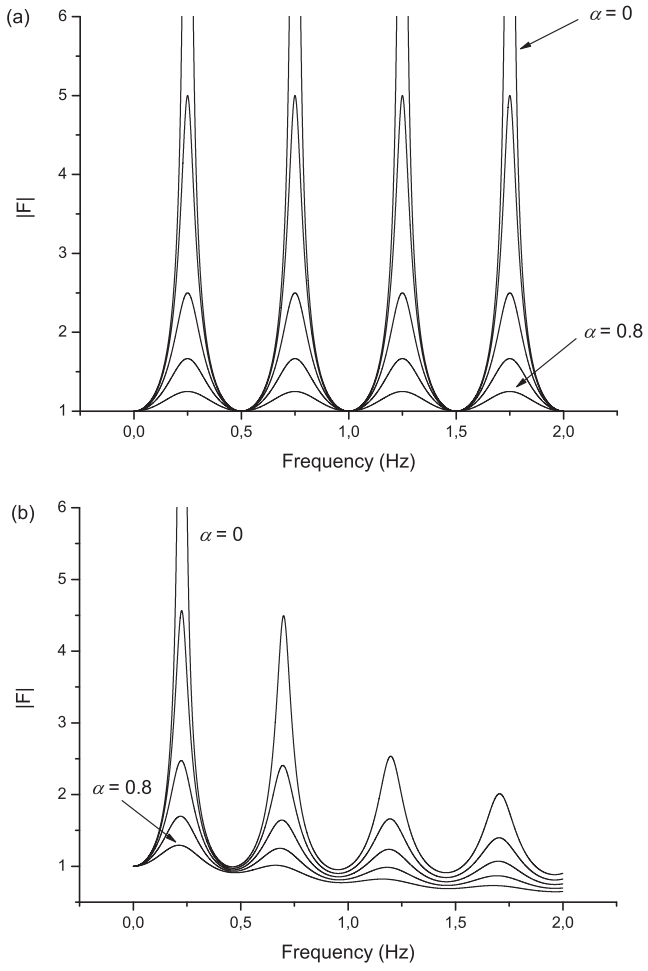

Figure 6. Amplification in the lossless (a) and lossy (b) cases for different values of the impedance contrast α (0, 0.2, 0.4, 0.6 and 0.8), corresponding to the fundamental and higher modes. In (a) it is $Q_1 = Q_2 = \infty$, while in (b) it is $Q_1 = 10$ and $Q_2 = 50$.

as the impedance contrast increases, that is, the separation between modes increases.

All these cases show a minimum of the transfer function at the fundamental frequency, as explained in Appendix A.

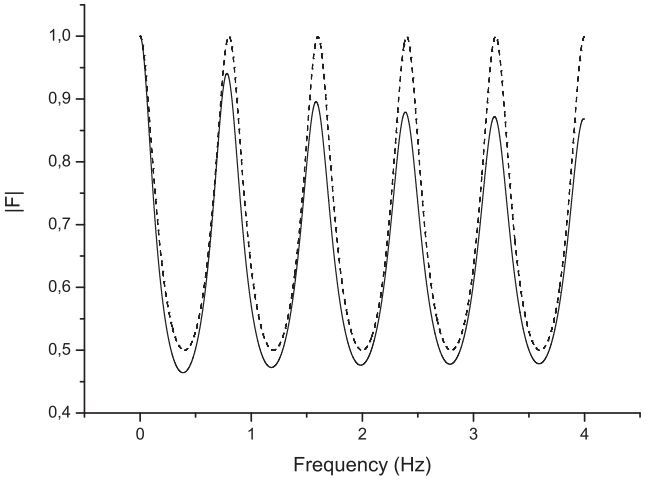

Figure 7. Amplification in the lossless case (dashed line, $Q_1 = 50$, $Q_2 = \infty$) and lossy case (solid line, $Q_1 = 50$, $Q_2 = 10$) for $\alpha = 2$. The lower half-space is softer than the layer, such that $c_{U1} = 1.6$ km s^{-1}, $\rho_1 = 2.5$ g cm^{-3}, $c_{U2} = 1$ km s^{-1} and $\rho_2 = 2$ g cm^{-3}.

3.3 Effects of the attenuation model

The effect of the frequency dependence of the attenuation is analysed by assuming a constant-Q model. This model has a simple expression of the complex velocity $v = c_U\sqrt{1 + \mathrm{i}/Q}$, such that the phase velocity and quality factor are frequency independent and equal to $1/\mathrm{Re}(1/v) > c_U$ and $\mathrm{Re}(v^2)/\mathrm{Im}(v^2) = Q$ over the whole frequency range. Since this velocity is greater than the lossless velocity c_U, it is expected a shift of the resonance peaks towards the high frequencies, that is, the opposite effect compared to the Zener model. However, no significant shift is observed with respect to the ideal lossless-rigid case, as can be seen in Fig. 10, corresponding to the lossy-elastic case represented in Fig. 2 (we assume the same values for Q, that is, $Q_1 = 10$ and $Q_2 = 50$). We can see that the modes have been attenuated compared to the Zener model.

As stated above, the location of the Zener relaxation peak affects the location of the fundamental mode. Fig. 11 displays the amplification function for the Zener relaxation peaks located at 0.05 Hz and 1 Hz, to the left and right of the fundamental mode in the lossless-rigid case. As can be seen, when the Zener relaxation peak is located at the left side, the shift is minimal, since the resonance modes 'see' the lossless velocity c_U.

It can be shown that in this case (rigid bedrock) there is no shift with respect to the ideal lossless-rigid case. Summarizing, the frequency dependence of the attenuation factor affects the amplitude and location of the modes, so that each case needs a specific calculation.

3.4 Real cases: Alpine glacier and Antarctic ice stream

We consider two real cases, with attenuation described by the constant-Q model (use of the Zener model yields similar results). Picotti *et al.* (2017) applied active seismic, radio echo sounding and geoelectric methods to verify the HVSR technique on Alpine glaciers and on a fast flowing ice stream of West Antarctica. In that work, the passive seismic measurements were carried out using different broadband seismometers, that is, a Guralp, a Lennartz and a Nanometrics. The H/V spectra were obtained by performing a statistical analysis of the recorded wavefield in the frequency domain using the free software GEOPSY (http://www.geopsy.org – SESAME Project), whose details can be found in Picotti *et al.* (2017). The

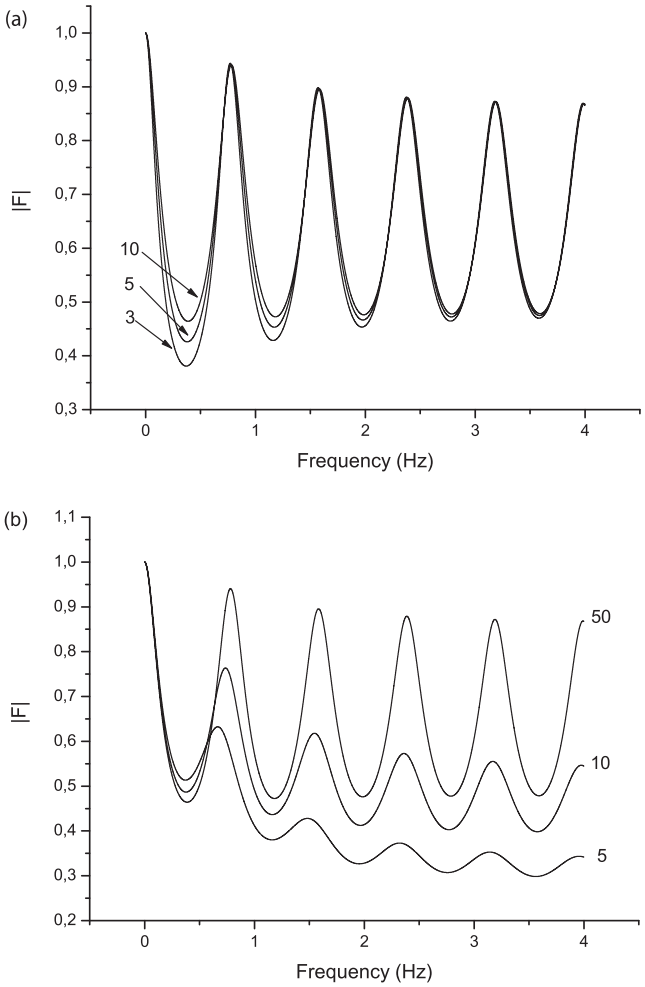

Figure 8. Amplification in the lossy case ($Q_1 = 50$ in (a) and $Q_2 = 10$ in (b)) for $\alpha = 2$. The number indicates the quality factor of the half-space (a) and layer (b), respectively.

software computes the amplitude spectra of the three components in a number of selectable time windows, whose width depends on the target frequency band and on the record length. The window selection criterion is based on the quasi-stationarity of the signal amplitude. For the computation of the H/V ratio, the amplitude spectra of the horizontal components are combined using vector summation. Picotti *et al.* (2017) compared the results obtained from different geophysical methods, showing that the resonance frequency in the H/V spectra can be well correlated with the ice thickness at the site, in a wide range from tens of metres to over 800 m. However, a theoretical interpretation of these results is required to understand how the H/V spectra change in the presence of a deformable basement. Here we consider two of the experiments of Picotti *et al.* (2017), carried out on the Pian di Neve glacier (Italy) and on the Whillans Ice Stream (WIS—West Antarctica).

The Pian di Neve glacier occupies a high altitude 18 km^2 plateau on the Lombardy side of the Adamello massif. In October 2014, a 1 km active multichannel seismic survey has been carried out on this glacier (Picotti *et al.* 2017) to image the bedrock and the basal moraine and to obtain the ice thickness profile. The imaging shows a smooth basement and the average thickness obtained from active seismic data is approximately $h = 250$ m. Picotti *et al.* (2017) also carried out several passive seismic experiments using different type of sensors in different seasons, reporting a good

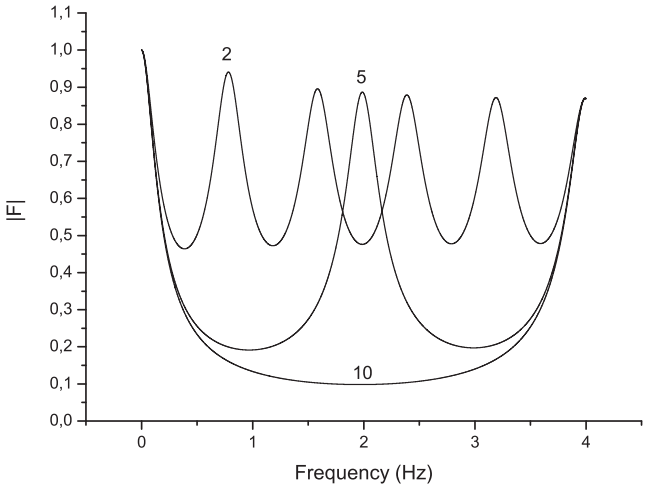

Figure 9. Amplification function in the lossy case for $\alpha = 2$, 5 and 10 ($Q_1 = 50$ and $Q_2 = 10$).

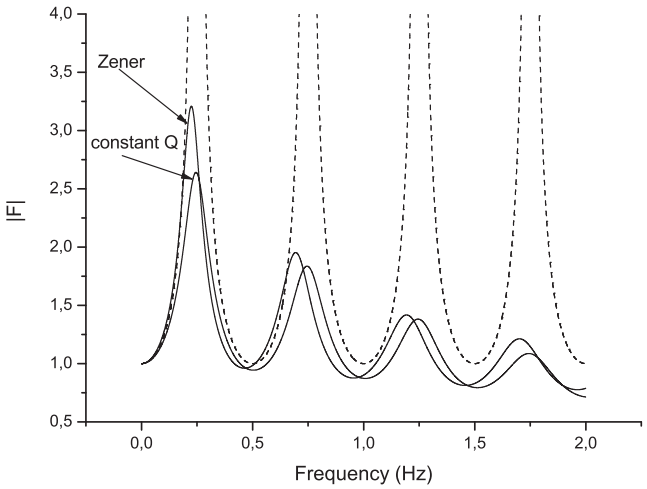

Figure 10. Amplification in the lossy-elastic (solid line, $Q_1 = 10$, $Q_2 = 50$, $\alpha = 0.3$). Attenuation is described by the Zener model and the constant-Q model (the two solid lines). The dashed line corresponds to the lossless-rigid case ($Q_1 = \infty$, $\alpha = 0$).

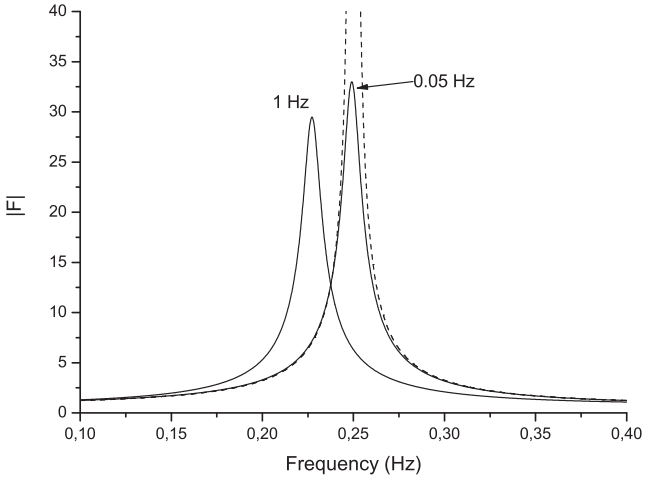

Figure 11. Amplification in the lossy-rigid (solid lines, $Q_1 = 10$, $\alpha = 0$) and lossless-rigid (dashed line, $Q_1 = \infty$, $\alpha = 0$) cases, corresponding to the fundamental mode. The numbers indicate the location of the Zener relaxation peak.

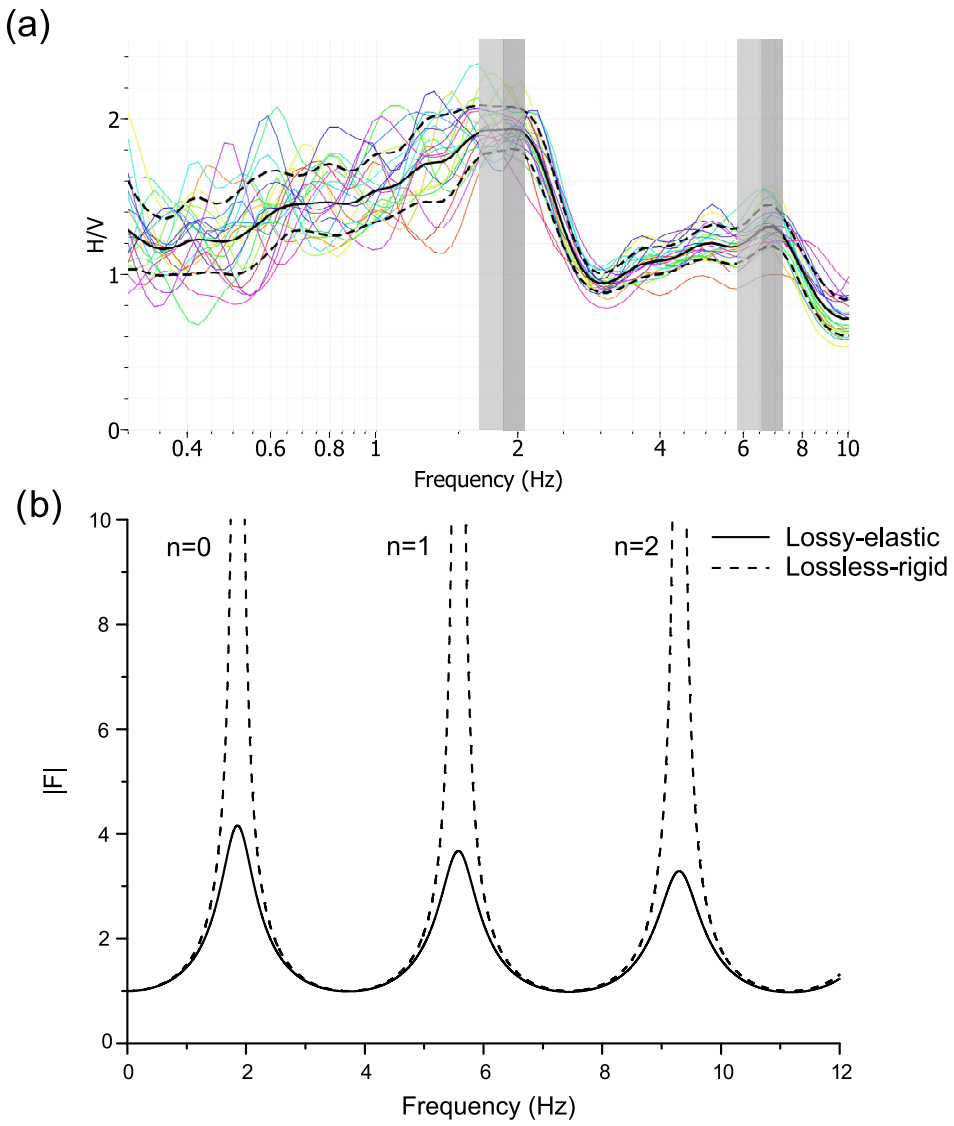

Figure 12. Experimental H/V response (a) and theoretical amplification functions (b) corresponding to the Pian di Neve glacier (Adamello massif, Northen Italy). The grey vertical bars quantify the experimental error associated to the resonance frequency of the fundamental (1.85 ± 0.3 Hz) and first higher modes (6.54 ± 0.7 Hz). The theory predicts the measured resonance frequencies both for the lossy-elastic and lossless-rigid models.

stability of the measured fundamental resonant frequency in the H/V spectra. Under the hypothesis of an underlying rigid bedrock, they show a good correspondence between the thickness obtained from the resonance frequency and that obtained from the imaging. Here we want to verify, in this case, the reliability of the lossless-rigid assumption.

The average *P*-wave velocity of the bedrock (4500 m s^{-1}) obtained from the imaging is consistent with the *in situ* rock types, which consist mainly of granitoid plutons compatible with the quartz-diorite (Blundy & Sparks 1992). Typical values of the *P*- to *S*-wave velocity ratio R_v for such fractured crystalline basins is around 1.6 (Moos & Zoback 1983), which yields an *S*-wave velocity for the bedrock of about $c_{U2} = 2812$ m s^{-1}. Moreover, the average density and quality factor of the bedrock can be assumed to be about 2700 kg m^{-3} (Hughes 1982) and $Q_2 = 150$ (Lay & Wallace 1995), respectively. The average ice density is $\rho_1 = 917$ kg m^{-3}, while the average *S*-wave velocity in ice, obtained from the active seismic method is approximately $c_{U1} = 1860$ m s^{-1} (Picotti *et al.* 2017).

A reliable approximation of the *S*-wave quality factor in ice can be computed using the following relationship

$$Q_1 = \frac{4}{3}\frac{Q_P}{R_v^2} \tag{5}$$

(Waters 1978; Udias 1999), where the *P*-wave quality factor Q_P in ice ranges from 70 to 200 in temperate environments (Peters *et al.* 2012). Considering that the value of R_v for ice determined by Picotti *et al.* (2017) on the Pian di Neve glacier is about 2, the local average *S*-wave quality factor in ice can be assumed $Q_1 \approx 50$. Fig. 12 shows the experimental H/V response (a) and the theoretical amplification function for the first three modes (b) using the lossy-elastic and lossless-rigid models. The coloured curves in Fig. 12(a) represent the H/V spectra obtained in each window selected for the statistical analysis. The thick black curve represents the H/V spectrum obtained as geometrical average of all the coloured H/V curves. The two dashed lines represent the H/V standard deviation, while the grey areas represent the peak frequency standard deviation

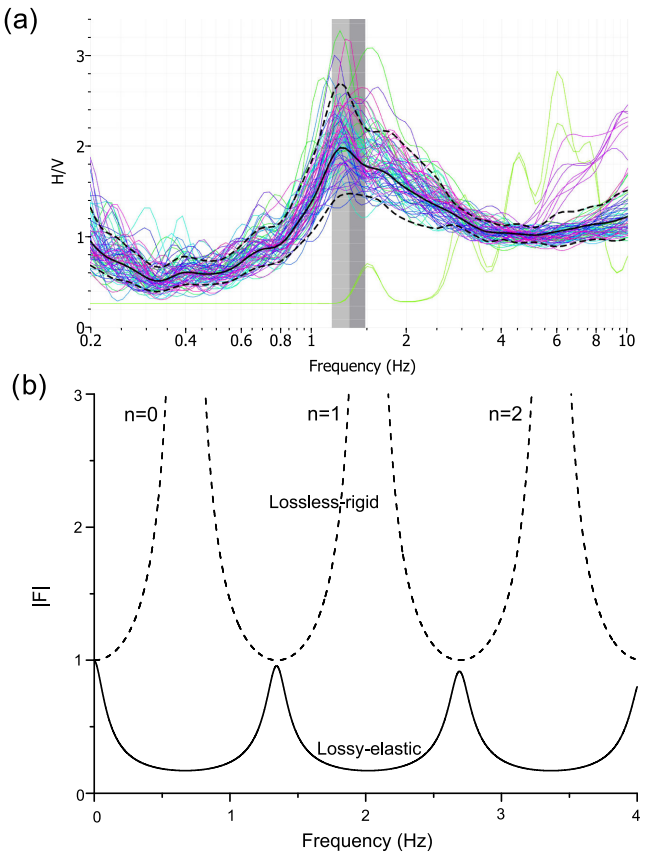

Figure 13. Experimental H/V response (a) and theoretical amplification functions (b) corresponding to the Whillans Ice Stream (West Antarctica). The grey vertical bars quantify the experimental error associated to the resonance frequency of the fundamental mode (1.3 ± 0.2 Hz). The theory predicts the measured fundamental-mode resonance frequency only for the lossy-elastic model.

and quantify the experimental error associated to the average peak frequency value (located at the limit between the dark and light grey areas). The relevant result is that for both the two considered models the theory agrees, within the experimental errors, with the measured fundamental resonance frequency given by the H/V peak. On the other hand, the modelled higher modes shown in Fig. 12(b) are damped with respect to the fundamental mode. Differences can be due to contributions of surface waves and to the fact that the H/V response is not the amplification function in terms of amplitudes. However, the discrepancy is very small and, in this case, the lossless-rigid assumption used by Picotti *et al.* (2017) for the computation of the glacier thickness is valid. Moreover, the measured data show a second peak at ≈6 Hz, which corresponds to the first higher mode according to Fig. 12(b).

The second real example is the WIS, a fast flowing ice stream feeding the Ross Ice Shelf from the interior of the West Antarctic Ice Sheet. Active seismic experiments (e.g. Blankenship *et al.* 1986; Picotti *et al.* 2015), as well as glaciological drilling and recordings (Engelhardt & Kamb 1997), show the presence of highly deformable sediments and water beneath the WIS. These experiments also discovered the presence of Subglacial Lake Whillans (Horgan *et al.* 2012; Tulaczyk *et al.* 2014). Picotti *et al.* (2017) analysed the H/V spectra obtained from the three-component seismic data recorded on the WIS by Picotti *et al.* (2015). The spectra show an average resonance peak at approximately 1.3 Hz. However, contrary to the previous case, the hypothesis of underlying rigid bedrock cannot be used to relate this frequency to the average ice thickness. Here we want to show that, in this case, the lossless-rigid assumption is actually inappropriate.

The thickness of WIS at the survey location is $h = 780$ m (Horgan *et al.* 2012), while the shallow firn layer is about 60 m thick (Picotti *et al.* 2015), indicating that the average ice thickness below the firn is approximately 720 m. Moreover, the ice stream has $c_{U1} = 1940$ m s^{-1}, $\rho_1 = 917$ kg m^{-3} and $R_v = 1.97$ (Picotti *et al.* 2015). Because in West Antarctica the ice Q_P ranges from 400 to 700 (Peters *et al.* 2012), it follows from eq. (5) that the local average *S*-wave quality factor can be assumed $Q_1 \approx 200$. Blankenship *et al.* (1986) show that the *S*-wave velocity and density of the sediments below the WIS are approximately $c_{U2} = 150$ m s^{-1} and $\rho_2 = 2016$ kg m^{-3}, respectively, which are compatible with a highly dilated and deforming material. The quality factor of such soft sediments can be assumed $Q_2 \approx 10$ (Lay & Wallace 1995). Fig. 13 shows the experimental H/V response (a) and theoretical amplification function for the first three modes (b) using the lossy-elastic and lossless-rigid models. Again, the modelled higher modes are damped with respect to the fundamental mode, but attenuation does not affect the resonance frequencies (i.e. the peak positions) significantly.

Contrary to the previous case, the theory predicts the measured H/V peak only for the lossy-elastic model. In fact, Fig. 13(b) shows that adopting the lossless-rigid approximation, the fundamental-mode frequency is approximately 0.68 Hz, well outside the experimental error bounds. As explained in Appendix A and shown in Section 3.2, this is due to the fact that when $\alpha \geq 1$ (stiff over soft medium) we have a minimum of the transfer function at the fundamental frequency f_0, and the first maximum is at $f_1 = 2f_0$. Thus, in this case assuming f_0 located at the H/V peak (i.e. using the lossless-rigid approximation) will result in a wrong estimation of the glacier thickness.

4 CONCLUSIONS

We studied the effects of soil and bedrock anelasticity on the *S*-wave amplification function, that is, how attenuation and bedrock deformability affect the amplitude and frequency of the resonance peaks. The Zener model is used to describe attenuation, with a single relaxation peak. We consider two different cases to study the location and amplitude of the fundamental mode, namely, the soil is softer than the bedrock (e.g. sediment over hard rock) and the layer is stiffer than the half-space (e.g. basalt over sediment).

In the first case, the presence of loss in the soil causes a shift of the peak towards the low frequencies, where the amount of shift depends on the location of the Zener relaxation peak compared to the fundamental-mode resonant frequency. Damping is caused either by attenuation or by elasticity of the bedrock, with the last effect dominating. Damping of the higher modes is noticeable when there is strong attenuation, mainly that of the layer. However, the half-space elasticity affects uniformly all the modes, that is, their amplitudes are similar. In the second case (softer bedrock with a given impedance), the modes shift to the higher frequencies and the spectrum stretches as the impedance contrast increases, that is, the separation between modes increases. Moreover, the transfer function shows a minimum at the fundamental frequency.

To analyse the effect of the frequency dependence of attenuation, we have considered a constant Q model. It is shown that the attenuation model affects the amplitude and location of the modes, so that each case needs a specific calculation. Finally, we consider

two real cases representing a glacier in Northern Italy and an ice stream in the Antarctic continent. These two examples, in which the upper layer is ice, show the prediction capabilities of the theory. In the latter case a very soft half-space (sediment) below ice yields a minimum at the fundamental frequency and a resonance peak at higher frequencies compared to a rigid half-space. Therefore, attenuation and bedrock elasticity must be considered to obtain reliable estimations of the layer thickness.

ACKNOWLEDGEMENTS

This work was supported by the Italian National Program of Antarctic Research (PNRA–WISSLAKE Project) and the U.S. National Science Foundation (WISSARD Program–NSF 0944794, 0632198, and 0424589). We would like to thank Alessandro Vuan for his constructive suggestions.

REFERENCES

Albarello, D. & Lunedei, E., 2011. Structure of ambient vibration wavefield in the frequency range of engineering interest ([0.5,20] Hz): insights from numerical modelling, *Near Surf. Geophys.,* **9,** 543–559.

Blankenship, D.D., Bentley, C.R., Rooney, S.T. & Alley, R.B., 1986. Seismic measurements reveal a saturated porous layer beneath an active Antarctic ice stream, *Nature,* **322,** 54–57.

Blundy, J.D. & Sparks, R.S.J., 1992. Petrogenesis of mafic inclusions in granitoids of the Adamello Massif, Italy, *J. Petrol.,* **33**(5), 1039–1104.

Bonnefoy-Claudet, S., Cornou, C., Bard, P.Y., Cotton, F., Moczo, P., Kristek, J. & Fäh, D., 2006. H/V ratio: a tool for site effects evaluation. Results from 1-D noise simulations, *Geophys. J. Int.,* **167**(2), 827–837.

Carcione, J.M., 2014. *Wave Fields in Real Media: Wave Propagation in Anisotropic, Anelastic, Porous and Electromagnetic Media,* 3rd edn, revised and extended, Elsevier.

D'Amico, V., Picozzi, M., Baliva, F. & Albarello, D., 2008. Ambient noise measurements for preliminary site-effects. Characterization in the urban area of Florence, *Bull. seism. Soc. Am.,* **98,** 1373–1388.

Engelhardt, H. & Kamb, W.B., 1997. Basal hydraulic system of a West Antarctic ice stream: constraints from borehole observations, *J. Glaciol.,* **43**(144), 207–230.

García-Jerez, A., Luzón, F., Sánchez-Sesma, F.J., Lunedei, E., Albarello, D., Santoyo, M.A. & Almendros, J., 2013. Diffuse elastic wavefield within a simple crustal model. Some consequences for low and high frequencies, *J. geophys. Res.,* **118,** 1–19.

Horgan, H.J., Anandakrishnan, S., Jacobel, R.W., Christianson, K., Alley, R.B., Heeszel, D.S., Picotti, S. & Jacob, I.W., 2012. Subglacial Lake Whillans—seismic observations of a shallow active reservoir beneath a West Antarctic ice stream, *Earth planet. Sci. Lett.,* **331–332,** 201–209.

Hughes, C.J., 1982. *Igneous Petrology,* Elsevier, p. 551

Kawase, H., Sánchez-Sesma, F.J. & Matsushima, S., 2011. The Optimal use of horizontal-to-vertical spectral ratios of earthquake motions for velocity inversions based on diffuse-field theory for plane waves, *Bull. seism. Soc. Am.,* **101,** 2001–2014.

Kawase, H., Matsushima, S., Satoh, T. & Sánchez-Sesma, F.J., 2015. Applicability of theoretical horizontal-to-vertical ratio of microtremors based on the diffuse field concept to previously observed data, *Bull. seism. Soc. Am.,* **105,** 3092–3103.

Konno, K. & Ohmachi, T., 1998. Ground-motion characteristics estimated from spectral ratio between horizontal and vertical components of microtremor, *Bull. seism. Soc. Am.,* **88**(1), 228–241.

Kramer, S.L., 1996. *Geotechnical Earthquake Engineering*. Prentice Hall.

Lay, T. & Wallace, T.C., 1995. *Modern Global Seismology,* Academic Press, p. 517

Lermo, J. & Chávez García, F., 1993. Site effect evaluation using spectral ratios with only one station, *Bull. seism. Soc. Am.,* **83**(5), 1574–1594.

Lunedei, E. & Albarello, D., 2015. Horizontal-to-vertical spectral ratios from a full-wavefield model of ambient vibrations generated by a distribution of spatially correlated surface sources, *Geophys. J. Int.,* **201,** 1142–1155.

Lunedei, E. & Malischewsky, P., 2015. A review and some new issues on the theory of the H/V technique for ambient vibrations, Chapter 15, in *Perspectives on European Earthquake Engineering and Seismology, Geotechnical, Geological and Earthquake Engineering,* Vol. 39, ed. Ansal, A., doi:10.1007/978-3-319-16964-4_15.

Moos, D. & Zoback, M.D., 1983. In situ studies of velocity in fractured crystalline rocks, *J. geophys. Res.,* **88**(B3), 2345–2358.

Nogoshi, M. & Igarashi, T., 1971. On the amplitude characteristics of microtremor (part 2), *Zisin, J. Seismol. Soc. Japan,* **24,** 26–40.

Peters, L.E., Anandakrishnan, S., Alley, R.B. & Voigt, D.E., 2012. Seismic attenuation in glacial ice: a proxy for englacial temperature, *J. geophys. Res.,* **117,** F02008, doi:10.1029/2011JF002201.

Picotti, S., Vuan, A., Carcione, J.M., Horgan, H.J. & Anandakrishnan, S., 2015. Anisotropy and crystalline fabric of Whillans Ice Stream (West Antarctica) inferred from multicomponent seismic data, *J. geophys. Res.,* **120**(6), 4237–4262.

Picotti, S., Francese, R., Giorgi, M., Pettenati, F. & Carcione, J.M., 2017. Estimation of glacier thicknesses and basal properties using the horizontal-to-vertical component spectral ratio (HVSR) technique from passive seismic data, *J. Glaciol.,* in press.

Sánchez-Sesma, F.J. *et al.*, 2011. A theory for microtremor H/V spectral ratio: application for a layered medium, *Geophys. J. Int.,* **186,** 221–225.

Takahashi, R. & Hirano, K., 1941. Seismic vibrations of soft ground (in Japanese), *Bull. Earthq. Res. Inst.,* **19,** 534–543.

Tulaczyk, S. *et al.*, 2014. WISSARD at Subglacial Lake Whillans, West Antarctica: Scientific operations and initial observations, *Ann. Glaciol.,* **55**(65), 51–58.

Udias, A., 1999. *Principles of Seismology,* Cambridge Univ. Press.

van der Baan, M., 2009. The origin of SH-wave resonance frequencies in sedimentary layers, *Geophys J. Int.,* **178**(3), 1587–1596.

Waters, K.H., 1978. *Reflection Seismology,* John Wiley and Sons, Inc.

APPENDIX A: ANALYSIS OF THE TRANSFER FUNCTION AT THE FUNDAMENTAL FREQUENCY

Let us consider the transfer function (2) in the lossless case and analyse its behaviour at the fundamental frequency. Its absolute value is

$$|F| = \left(\cos^2\beta + \alpha^2 \sin^2\beta\right)^{-1/2}, \quad \beta = \frac{\omega h}{v_1}, \tag{A1}$$

where α is given in eq. (4). We have

$$\frac{\mathrm{d}|F|}{\mathrm{d}\omega} = -\frac{h}{2v_1}\left(\cos^2\beta + \alpha^2\sin^2\beta\right)^{-3/2}(\alpha^2 - 1)\sin 2\beta. \tag{A2}$$

The location of the fundamental mode is obtained for $\mathrm{d}|F|/\mathrm{d}\omega = 0$, and it is

$$f_0 = \frac{v_1}{4h}. \tag{A3}$$

The second-order derivative at f_0 is

$$\frac{\mathrm{d}^2|F|}{\mathrm{d}\omega^2} = \left(\frac{h}{v_1}\right)^2 \frac{\alpha^2 - 1}{\alpha^3}. \tag{A4}$$

Then if $\alpha \leq 1$, we have a maximum (soft over stiff medium) and $\alpha \geq 1$ gives a minimum (stiff over soft medium). On the other hand, it can easily be shown that $|F| = 1$ at $f_1 = 2f_0$.